Title: Supramolecular Photoinduced Electron Transfer between A Redox-Active Hexanuclear Metal-Organic Cylinder and Encapsulated Ruthenium(II) Complex

Authors: Cheng He; Lu Yang; Xin Liu; Jing Zhang; Hui Sun; Huimin Guo

To be cited as: 10.1002/chem.201504975

Link to VoR: http://dx.doi.org/10.1002/chem.201504975

Supramolecular Photoinduced Electron Transfer between A Redox-Active Hexanuclear Metal-Organic Cylinder and Encapsulated Ruthenium(II) Complex

Lu Yang, Cheng He*, Xin Liu, Jing Zhang, Hui Sun and Huimin Guo*

Abstract: Using the redox-active nickel(II) ions as the connect nodes, a hexanuclear metal-organic cylinder (Ni–**YL**) was achieved via self-assembly with large cavity and opening windows capable to accommodate guests. The suitable cavity of Ni–**YL** provides an opportunity to encapsulate the anionic ruthenium-bipyridine derivative $Ru(dcbpy)_3$ (dcbpy = 2,2'-bipyridine-4,4'-dicarboxylicacid) as the photosensitizer for light driven reactions. The host-guest behavior between Ni–**YL** and $Ru(dcbpy)_3$ was investigated by mass spectra, NMR spectroscopy, and computational studies, revealing the effective binding of the guest $Ru(dcbpy)_3$ within the cavity of Ni–**YL**. Optical experiments suggested a pseudo-intramolecular photoinduced electron transfer (PET) between the $Ru(dcbpy)_3$ and the host Ni–**YL** leading to the efficient light driven hydrogen production based on this system. Control experiments with a mononuclear Ni complex as a reference photocatalyst and the inactive $Fe(dcbpy)_3$ as an inhibitor for comparison were also performed to confirm such a suprmolecular photocatalysis process.

Introduction

Binding the specific guest molecules within the cavity of host molecules is one of the classical issues which have drawn continuous attentions in the supramolecular chemistry.[1] The hosts can be well-modified with functional interaction sites and well-defined inner void spaces by ingenious design and construction, usually defined as molecular containers for their ability to accommodate other chemical species.[2,3] The excellent and well-studied hosts in this field were mainly focus on macrocycles formed *via* covalent bonds, including the cyclodextrins, calixarenes, covalent capsules and cucurbiturils, which have been widely delineated by the pioneering work of many groups.[4] During the last decades, another kind of interesting molecular hosts, the coordination driven self-assembled metal-organic polyhedra (MOPs) containing internal cavities with well-defined shapes and sizes, have achieved increasing prominence.[5] Owing to their promising functionalities as artificial metalated host platforms, it is possible for these molecular hosts to mimic protein receptors or enzymes for their abilities to effectively bind substrates, stabilize reactive intermediates, and catalyze chemical transformations.[6]

On the other hand, a rising interest in reactions driven by the photoinduced electron transfer (PET), in particular, for the production of solar fuels, presents opportunities to design new systems that absorb visible light and exhibit favorable redox chemistry for photo-sensitization. The construction of the host–guest supramolecular photosynthetic systems would enforce the electron transfer process in a local microenvironment,[7] thus the pseudo-intramolecular electron and energy transfer could be modified to avoid unwanted electron transfer processes. In this case, the introduction of metal ions would endow metallosupramolecular hosts excellent redox-active property for the PET process, together with their benign host-guest behavior, that the MOP system could act as a kind of potential model in photoredox reactions.[8]

Herein, we report a new cationic hexanuclear metal-organic cylinder (Ni–**YL**) as a host for the encapsulation of anionic trisbipyridine ruthenium derivative, by incorporating the Ni(II) ions as construction nodes and the flexible **YL** ligand containing amide and secondary amino groups as trigger sites (Figure 1a). Tris(bipyridine) ruthenium(II) complexes and its derivatives are well-known for their excellent photophysical and excited-state redox properties.[9] The encapsulation of such complexes within the well-designed supramolecular system could bring fruitful applications in the photochemical field. We envisioned that the extremely flexible backbone and the large cavity of the host, couple with the potential hydrogen bonding interactions would provide an opporatunity to construct suitable architecture to encapsulate this widely used photosenstizer. And the introduction of the well-coordinated nickel ion as the connect nodes was expected to exhibit suitable redox-active property for proton reduction and the complexation species greatly improved the efficiency of proton transfer within the well-defined microenvironment.

Results and Discussion

The backbone of **YL** ligand contains three amide groups and one secondary amine group that linked by 4-carbohydrazide and 5-amino-isocarbohydrazidebenzene. The ligand was prepared by the reaction of the 5-(4-(hydrazinecarbonyl)benzylamino)isophthalohydrazide with 2-pyridinecarboxaldehyde under the reflux in methanol. Vapour diffusion of diethyl ether into the mixture of ligand and $Ni(BF_4)_2{\cdot}6H_2O$ in acetonitrile led to the crystallization of the cylinder Ni–**YL**. ESI-MS spectrum of Ni–**YL** in acetonitrile solution exhibits four main bunches of peaks at *m/z* = 923.80,

[*] Ms. L. Yang, Prof. C. He, Dr. X. Liu, Ms. J. Zhang, Mr. H. Sun and Dr. H. Guo
State Key Laboratory of Fine Chemicals,Dalian University of Technology,Dalian, 116023, P. R. China
Fax: (+86)-411-84986261
E-mail: guohm@dlut.edu.cn; hecheng@dlut.edu.cn

Supporting information for this article is given via a link at the end of the document.

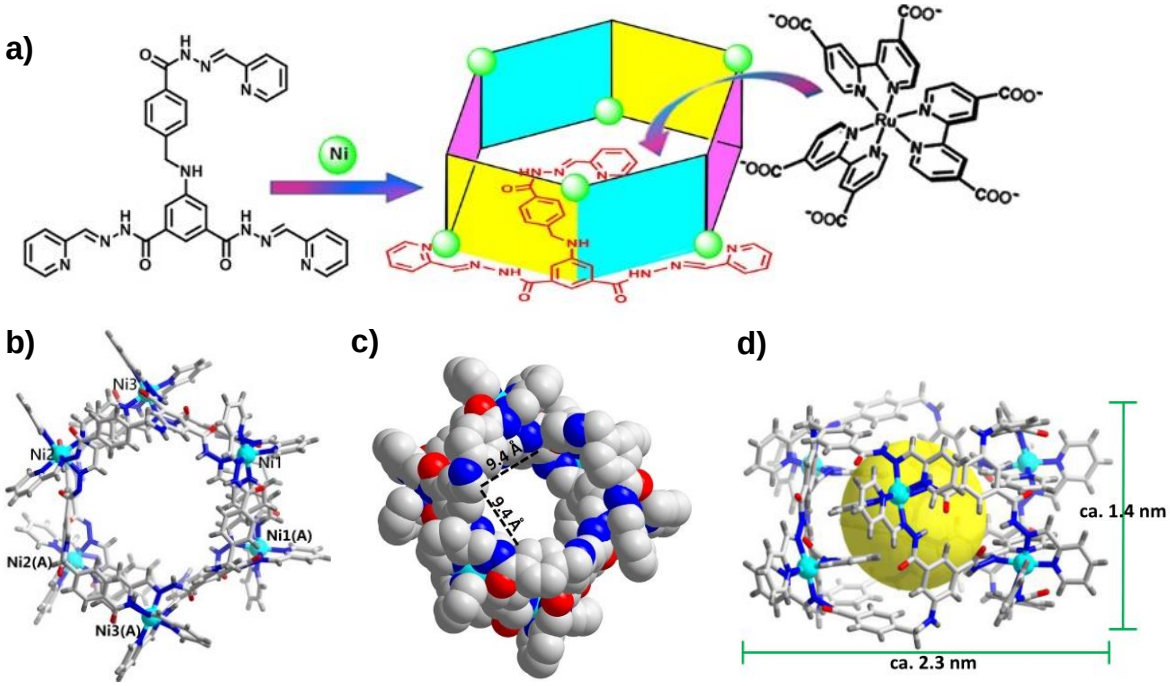

Figure 1. a) Representation of the assembly of metal-organic cylinder Ni–**YL** host and the encapsulation of the anionic $Ru(dcbpy)_3$ via host-guest behavior; b) Molecular structure of Ni–**YL** from the top view; c) The space-filling representation of the vast cavity of cylinder Ni–**YL**; d) The side view of Ni–**YL**. Solvent molecules and anions are omitted for clarity. The metal, oxygen, nitrogen and carbon atoms are drawn in cyan, red, blue and grey, respectively. Symmetry code A: -x-1,-y-1,z.

941.40 1176.25 and 1198.25, assigned to the species $[Ni–\mathbf{YL}\cdot6(BF_4)]^{5+}$, $[Ni–\mathbf{YL}\cdot7(BF_4)]^{5+}$, $[Ni–\mathbf{YL}\cdot7(BF_4)]^{4+}$ and $[Ni–\mathbf{YL}\cdot8(BF_4)]^{4+}$, respectively. This result suggested that the formation and stable existence of a Ni_6L_6 complex in solution. Single crystal X-ray diffraction revealed that the assembly of six Ni(II) ions and six ligands formed the large cationic hexanuclear cylinder Ni–**YL** approximately with the length of 2.3 nm and the height of 1.4 nm (Figure 1). All the three-armed ligands connect to three different nickel ions, while the six nickel ions each coordinate with three different ligands as the NN bidentate chelators in an octahedral geometry. Thus, the amide groups are coordinated free due to the rotation of the C=O bond, unlike with the previous reported ligands of amide groups involved tridentate chelators by our group.[10] The flexible ligand can be represented as a tripod with the central secondary amine group as the vertex. One arm of a ligand is bound to one Ni ion in one layer, while the other two arms are connected to two ions in the other layer. From the side view of the cylinder, the six nickel ions are positioned at two different layers that are formed by three of the coplanar nickel ions, and the three nickel ions in the same layer present triangle configuration with the average edge distance of 14.7~15.1 Å. The distances of C=O and C−N bonds in the ligand backbone are intermediate between formal single and double bonds, suggesting the extensive delocalization over the whole skeleton.[11]

Notably, the structure of Ni–**YL** is similar to the classic covalent host cucurbit[6]uril molecule and its derivatives, both of which are hexameric species and possess cylindrical cavities. The cucurbit[6]uril molecule contains twelve high active C=O groups sequentially arranged along the margins of the cylinder exhibiting the binding ability toward the substrate.[12] While in Ni–**YL**, there are eighteen free amide groups and six secondary amines which could act as hydrogen bonding interaction sites. Moreover, the openning window of Ni–**YL** cavity is about 9.4 Å (Figure 1c), much larger than that of cucurbit[6]uril molecule (5.8 Å) and even comparable to the diameter of cucurbit[8]uril molecule which is 8.9 Å. But the external diameters of Ni–**YL** and cucurbit[6]uril are close to each other showing that Ni–**YL** possesses broader opening window to accommodate the guests to access. The positively charged cylinder could provide restrained inner space to the capsules, together with the rotatable secondary amine groups and intact amide groups that acting as possible hydrogen bond interaction sites. Thus, we expected that Ni–**YL** was shown to be a promising metal-organic macrocycle host, like those of the cucurbit[6]uril molecule and its derivatives,[13] possessing high host-guest behavior with high affinity and selectivity toward the specific substrates.[14]

The carboxylic derivative of tris(bipyridine) ruthenium(II), $Ru(dcbpy)_3$ represents an ideal guest in our system not only because of its appropriate size and excellent photophysical properties, but also based on the fact that it exists in an anion form in alkaline medium that could interact with the positive-charged host driven by electrostatic attraction. The host-guest behavior of binding $Ru(dcbpy)_3$ was firstly investigated by ESI spectrum. The addition of equimolar amount $Ru(dcbpy)_3$ into the acetonitrile solution of Ni–**YL** in the presence of TEOA exhibited

several new peaks at *m/z* = 1072.60, 1090.20, 1340.50 and 1384.50 (marked with red asterisk). Compared the simulation results based on natural isotopic abundances, these peaks were assigned to $[Ni–\mathbf{YL}·Ru(dcbpy)_3·4(BF_4)]^{5+}$, $[Ni–\mathbf{YL}·Ru(dcbpy)_3·6(BF_4)]^{5+}$, $[Ni–\mathbf{YL}·Ru(dcbpy)_3·5(BF_4)]^{4+}$ and $[Ni–\mathbf{YL}·Ru(dcbpy)_3·7(BF_4)]^{4+}$, respectively (Figure 2), confirming the formation of a 1:1 stoichiometric complexation species $[Ni–\mathbf{YL}·Ru(dcbpy)_3]$. Moreover, the ^{1}H-NMR titration of $Ru(dcbpy)_3$ (Figure S8) also in CD_3CN and D_2O (v = 1:1) upon addition of 1 mole ratio Ni–**YL** in above solution exhibited the significant downfield shifts of protons ($\Delta\delta$ = 0.19, 0.45 and 0.04 *ppm*, respectively). These shifts provide another indicator for the encapsulation of the anionic $Ru(dcbpy)_3$ within the suitable pocket of the cylinder Ni–**YL** forming the host-guest complexation species $Ru(dcbpy)_3\subset$Ni–**YL**.

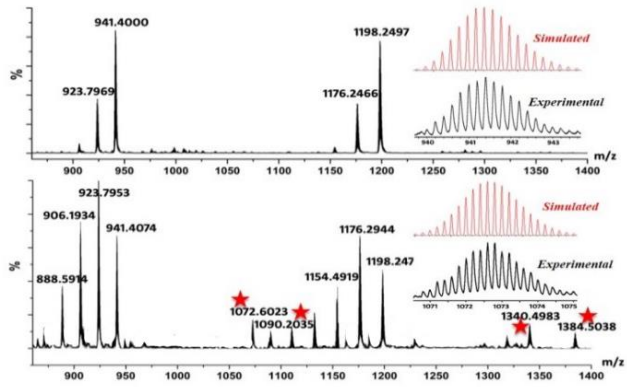

Figure 2. ESI-MS spectra of Ni–**YL** in acetonitrile solution (top) and of $Ru(dcbpy)_3$ in methanol solution mixed with aforementioned solution (bottom). The inserts show the measured and simulated isotopic patterns at m/z = 941.4000 (top) and 1072.6023 (bottom), respectively.

Extensive molecular force field-based calculations were performed to get a possible picture of the cationic Ni–**YL** cylinder and the $Ru(dcbpy)_3\subset$Ni–**YL** encapsulation starting from the crystal structure of Ni–**YL** and $Ru(dcbpy)_3$ in water solution using universal force field as implemented in Gaussian 09.[15] Frequency analysis was also carried out to ensure the calculated structures are real minimum on the potential energy surface (Figure 3). In the most plausible structure of Ni–**YL**, the averaged Ni−Ni distance is 14.90 Å falling in the experimental range of 14.7~15.1 Å and the diameter of the cavity on top of the cylinder is 9.78 Å with a diagonal of 17.62 Å. The large size of the cavity ensures the encapsulation of the $Ru(dcbpy)_3$, in which the largest O−O distance is 13.84 Å. There is no significant structure change observed on Ni–**YL** in the plausible structure of the encapsulation. In fact, the $Ru(dcbpy)_3$ fully utilizes the apertures on the side walls of Ni–**YL** to release the tension. At the same time, one of the dcbpy ligand is reoriented to be parallel to the neighboring **YL** ligand and the nearest distance is 3.75 Å which is typical for π-π stacking among aromatic molecules. At the same time, close contacts were also observed between the carboxyl groups of dcbpy and N−H on the Ni–**YL** and the nearest O–H distance is only 2.61 Å which is typical for hydrogen bonds. These interactions may each play a role in promoting the encapsulation thermodynamically and remaining the stable of the complexation. These results could relate to the NOESY spectrum of the mixture of $Ru(dcbpy)_3$ and Ni–**YL** with equal stoichiometric ratio, which indicates the interactions between H–H of the two components, namely the protons of the pyridine rings of the $Ru(dcbpy)_3$ and the skeleton of cylinder (red circles).

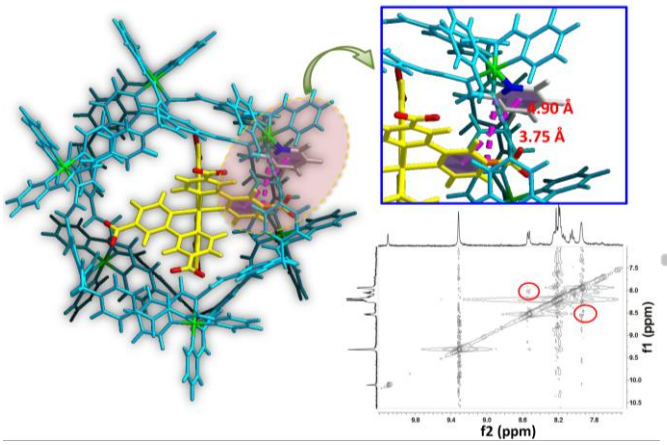

Figure 3. The representation of the encapsulation of Ni–**YL** and $Ru(dcbpy)_3$ computed by molecular force field-based calculations and partial NOESY spectrum of the two components in the mixture of D_2O and acetonitrile-d_3.

Cyclic voltammograms (CVs) of Ni–**YL** in acetonitrile solution displayed a Ni^{II}/Ni^{I} reduction wave at -0.75 V (vs. Ag/AgCl) with the scan rate of 100 $mV·s^{-1}$.[16] The addition of TEOA·HCl with increasing amounts triggers the appearance of a new irreversible wave near the Ni^{II}/Ni^{I} response (Figure 4a). Increasing the TEOA·HCl concentration raises the height of the new wave and shifts to more negative potentials while the Ni^{II}/Ni^{I} reversible wave disappeared. The new wave is assignable to the typical proton electroreduction, suggesting that Ni–**YL** is able to reduce proton through catalysis process. In order to construct stable host guest complexation species with the cationic host Ni–**YL**, the $Ru(dcbpy)_3$, which has suitable redox potential[17] in the basic condition, was chosen as the photosensitizer.

Fluorescence titration revealed that the addition of Ni–**YL** in the solution of $Ru(dcbpy)_3$ caused significant emission quenching (Figure 4b). The quenching process is easily attributed to a classical photoinduced electron transfer from the excited state *Ru(II) to the redox catalyst Ni–**YL**.[18] Ni–**YL** thus is able to be activated directly for the proton reduction by the excited state *Ru(II). Luminescence of a $Ru(dcbpy)_3$ solution (10.0 μM) at 620 nm containing Ni–**YL** (20.0 μM) decays in an exponential fashion with the lifetime of 1.06 μs similar to that of the free $Ru(dcbpy)_3$ solution (1.07 μs, Figure S13). It seems that two luminescent species coexist: the $Ru(dcbpy)_3$ moiety itself with its fluorescent lifetime being maintained, and the host-guest complexation species $Ru(dcbpy)_3\subset$Ni–**YL** in the titration mixture. The fact that decay behavior approximates well to a typical exponential function suggests that the complexation species

exhibits ignored emission. The titration profile of $Ru(dcbpy)_3$ (10.0 μM) upon addition of Ni–**YL** up to 50.0 μM is consistent with the Hill-plot.[7c] The best-fitting of the titration profile suggests a 1:1 host-guest behavior with the association constant (K_{ass}) as $6.46\pm0.13 \times 10^4$ M^{-1}.

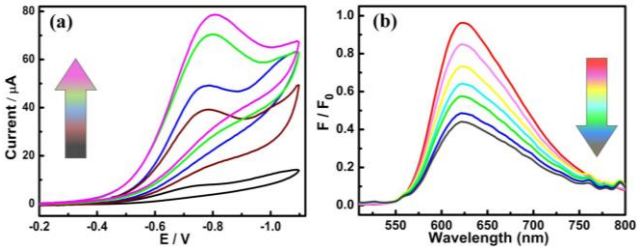

Figure 4. a) Cyclic voltammograms of Ni–**YL** (1 mM) upon addition of 2.0, 4.0, 6.0 and 8.0 ratio of TEOA·HCl in CH_3CN solution containing $TBAPF_6$ (0.1 M); b) The emission quenching of $Ru(dcbpy)_3$ (10.0 μM) upon the addition of Ni–**YL** in 1:1 EtOH/H_2O at pH 10.5.

In a typical light driven reduction system containing photocatalyst (Ni–**YL**), photsenzitizer $Ru(dcbpy)_3$ and electron donor (triethanolamine, TEOA), there are two possible reaction pathways. One of the pathways is the excited state of $*Ru(II)(dcbpy)_3$ being reduced by the TEOA to $Ru(I)(dcbpy)_3$ through a reductive quenching process, then the electron is transferred from $Ru(I)(dcbpy)_3$ specie to the Ni–**YL** catalyst and a possible proton reduction could occur on the catalyst. Another way is that the electron is directly transferred from the $*Ru(II)(dcbpy)_3$ to the catalyst Ni–**YL**, and the following step should be that the $Ru(III)(dcbpy)_3$ species were reduced by TEOA. Both the two processes are thermodynamically feasible in our system, the PET process of $Ru(dcbpy)_3$ (40.0 μM) with Ni–**YL** (40.0 μM) in the presence of TEOA (15 % in volume) was then investigated by transients absorption studies (Figure 5a, blue line). The spectrum recorded at 2.4 μs after laser flash showed a peak at 420 nm corresponding to the maximum absorption of Ru(III) ions,[19] and no absorption of Ru(I) ions was observed at 6 μs after laser flash, indicating the direct PET process from the excited state *Ru(II) to Ni(II) centres to form Ru(III) species was happened under this light driven condition.

To further investigate whether the existence of the supramolecluar species $Ru(dcbpy)_3$⊂Ni–**YL** indeed influence the PET process for light driven H_2 generation, a mononuclear complex Ni–**ML** exhibiting the similar coordination mode of Ni centre as with Ni–**YL** was synthesized as a reference (Figure 5d). The CV of Ni–**ML** revealed a reduction peak assignable to Ni^{II}/Ni^{I} process ($E_{1/2}$ = -0.78 V) exhibiting the similar redox potential with that of Ni–**YL**. The process of the fluorescence of $Ru(dcbpy)_3$ quenched by Ni–**ML** is consistent with the Stern-Volmer profile with the Stern-Volmer constant (K_{sv}) as $1.95\pm0.13 \times 10^3$ M^{-1} (Figure S12). The decrease of emission lifetime (from 1.07 to 0.86 μs) of $Ru(dcbpy)_3$ (10.0 μM) with addition of Ni–**ML** (0.12 mM) suggested that the photoinduced electron transfer displayed in a normal bimolecular manner. The transients absorption spectrum recorded at 2.4 μs after laser flash of $Ru(dcbpy)_3$ with Ni–**ML** could not find the characteristic absorption of Ru(III) ions, but at the 6 μs the absorption of Ru(I) ions was observed, demonstrating that an excited state reduction quenching of $Ru(dcbpy)_3$ by TEOA clearly dominates the light driven process.

From a mechanistic point of view, the encapsulated molecules of $Ru(dcbpy)_3$ inside the pocket of Ni–**YL** enforces the proximity between the nickel-based redox catalytic sites and the photosensitizer. This supramolecular system then allows a direct photoinduced electron transfer (PET) process from the excited state *Ru(II) to the redox catalyst.[20] The close proximity between the redox sites and the photosensitizer within the confined space further encourages the PET process in a more powerful pseudo intramolecular pathway.[21]

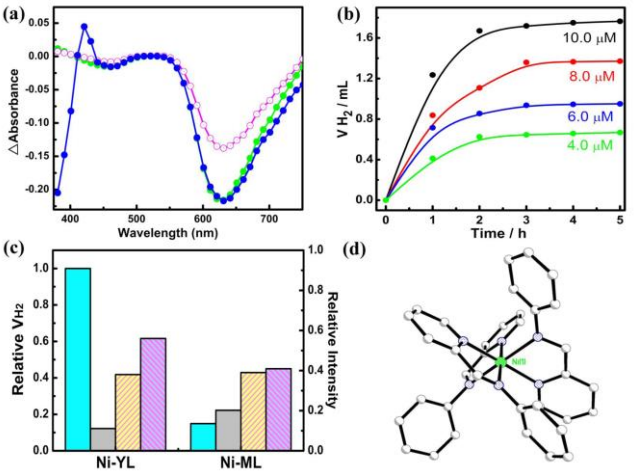

Figure 5. (a) Transient absorption spectra of $*Ru(dcbpy)_3$ (40.0 μM) in the presence of TEOA (15 %, pink) and Ni–**YL** (40.0 μM, blue) or Ni–**ML** (0.24 mM, green) in H_2O/EtOH (1:1 in v:v) solution at 298 K recorded at 2.4 μs after laser flash; (b) H_2 production upon the irradiation of the system containing TEOA (15 %), pH = 10.5 and $Ru(dcbpy)_3$ (2.0 mM) with different concentrations of Ni–**YL**; (c) Histogram of H_2 production upon the systems containing Ni–**YL** (10.0 μM) or Ni–**ML** (60.0 μM), respectively, TEOA (15 %) and $Ru(dcbpy)_3$ (2.0 mM) at pH=10.5 (cyan bar); and the addition of 2.0 mM $Fe(dcbpy)_3$ (gray bars) as inhibition; and the normalized emission intensity of 10.0 μM $Ru(dcbpy)_3$ (yellow bar) upon addition of Ni–**YL** (50 μM) or Ni–**ML** (0.3 mM), respectively, and of the recovery in the presence of 0.1 mM $Fe(dcbpy)_3$ for Ni–**YL**, 0.6 mM for Ni–**ML** (pink bars); Intensities were recorded at 620 nm, excitation at 470 nm; (d) Crystal structure of Ni–**ML**.

Irradiation of a solution containing $Ru(dcbpy)_3$ (2.0 mM), Ni–**YL** (10.0 μM), and TEOA (15 %) in a H_2O/ EtOH (1:1 in v:v) solution at 298 K resulted in a direct hydrogen generation. A common Xe lamp (500 W) was utilized as the light source using a 400 nm filter to eliminate the effect of ultraviolet lights. The highest efficiency of the H_2 production was achieved when the initial pH value was 10.5, while the ultimate pH value reduced to 10.2 after the irradiation. By fixing the concentrations of $Ru(dcbpy)_3$ (2.0 mM) and TEOA (15 %), the volume of the hydrogen produced holds a linear relationship with the concentrations of the catalyst Ni–**YL** ranging from 4.0 μM to 10.0 μM (Figure 5b). The initial turnover frequency (TOF) is about 1100 moles hydrogen per mole of catalyst per hour, and the

calculated turnover number (TON) is about 1600 moles hydrogen per mole of catalyst. This TON value was compared to some previously reported Ru/TM (transition-metal) system.[22] Control experiments suggested that the absence of any components could hardly trigger the process of proton reduction to H_2. When using the **YL** ligand (60.0 μM) or $Ni(BF_4)_2$ (60.0 μM) to replace the redox catalyst Ni–**YL**, no H_2 could be detected under the same reaction conditions.

An inhibition experiment was performed by adding a non-reactive species, $Fe(dcbpy)_3$, into the reaction mixture.[23] The volume of the hydrogen produced in the presence of $Fe(dcbpy)_3$ (2.0 mM) was only 12.2 % of that from the original system under the same experimental conditions (Figure 5c). Since the $Fe(dcbpy)_3$ did not quench the luminescence of the $Ru(dcbpy)_3$, the competitive inhibition behavior further confirmed that the PET process between $Ru(dcbpy)_3$ and Ni–**YL** occurred within the pocket of Ni–**YL** cylinder by a typical enzymatic fashion in a more efficient way.[24] It should also be noted that the addition of $Fe(dcbpy)_3$ (0.1 mM) to the solution mixture containing $Ru(dcbpy)_3$ (10.0 μM) and Ni–**YL** (50 μM) resulted in an emission recovery of the same band. Such a recovery of the emission of $Ru(dcbpy)_3$ also indicated the substitution of encapsulated $Ru(dcbpy)_3$ molecules in the pocket of the molecular cylinder Ni–**YL** by the inhibitor $Fe(dcbpy)_3$. When we irradiated the aforementioned $Ru(dcbpy)_3$(2.0 mM)/Ni–**ML** (60.0 μM)/TEOA (15 %) system, about 0.26 mL of hydrogen was produced after 5 hours irradiation. Besides, the addition of corresponding concentration $Fe(dcbpy)_3$ did not change much volumes of the hydrogen production, and also could hardly recover the emission intensity. These results indicate the advantage of the supramolecular system on this light driven reaction.

Conclusions

In summary, a hexanuclear metal-organic cylinder based on redox-active Ni(II) centres was prepared through the coordination of metal-organic assemblies. Owing to the introduction of amide groups and secondary amine groups, together with the design of fixable backbone, complex Ni–**YL** possesses a large cavity and diversified acting sites with the capability of encapsulating size-suitable anionic $Ru(dcbpy)_3$ showing obvious host-guest behavior in solution. Optical measurements and control experiments reaveal the pseudo-intramolecular PET between the $Ru(dcbpy)_3$ and the Ni–**YL** host which lead to the efficient light driven hydrogen production based on this system. These results suggest that our supramolecular system favorites the pseudo intramolecular PET process, showing the bright future as artificial photosynthetic systems for efficient photocatalytic reaction.

Experimental Section

Materials and Methods All chemicals were of reagent grade quality obtained from commercial sources and used without further purification. The photosensitizer $Ru(dcbpy)_3$ and $Fe(dcbpy)_3$ with the same configuration were prepared following the literature methods.[25,26] The elemental analyses of C, H and N were performed on a Vario EL III elemental analyzer. ^{1}H NMR spectra were measured on a Varian INOVA 500M spectrometer. ESI mass spectra were carried out on a HPLC-Q-Tof MS spectrometer using methanol as mobile phase. The solution fluorescent spectra were measured on JASCO FP-6500. Both excitation and emission slit widths were 5 nm. The solution of Ni–**YL** was prepared in CH_3CN solvents with the concentration of 1 mM. And stock solutions of $Ru(dcbpy)_3$ (1 mM) was prepared directly in methanol with some addition of NaOH to pH = 10.5 for the test of fluorescence titration and transient absorption. The electrochemical studies were measured on the CHI 1130 (CH Instrument Co., Shanghai) electrochemical analyzer under nitrogen at room temperature using Ag/AgCl electrode as a reference electrode, a platinum silk with 0.5 mM diameter as a counter electrode, and glassy carbon electrode as a working electrode. The nanosecond time-resolved transient difference absorption spectra were obtained using an Edinburgh LP920 instrument (Edinburgh Instruments, UK).

For photoinduced hydrogen evolution,[27] the system was irradiated by a 500 W Xenon lamp; the reaction temperature was 298 K by using a water filter to absorb heat. The flask was sealed with a septum and degassed by bubbling argon for 30 min under atmospheric pressure at room temperature. The pH of the system was adjusted to a specific pH by adding HCl or NaOH and was measured with a pH meter. The generated photoproduct of H_2 was characterized by GC 7890T instrument analysis using a 5 Å molecular sieve column (0.6 m × 3 mm), thermal conductivity detector, and nitrogen used as carrier gas. The amount of hydrogen generated was determined by the external standard method. Hydrogen in the resulting solution was not measured and the slight effect of the hydrogen gas generated on the pressure of the flask was neglected for calculation of the volume of hydrogen gas.

Preparation

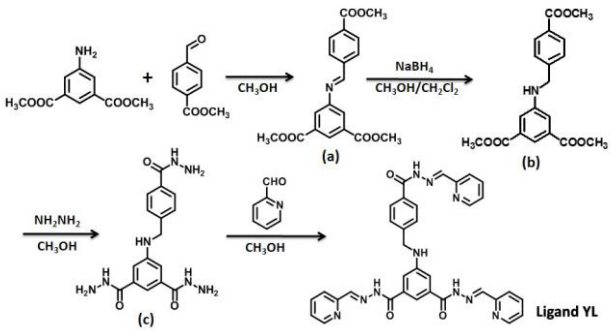

Scheme 2 Synthetic Routine of Ligand **YL**.

(*E*)-dimethyl 5-(4-(methoxycarbonyl)benzylideneamino)isophthalate (a): A mixture of dimethyl 5-aminoisophthalate (2.09 g, 10 mmol) and methyl 4-formylbenzoate (1.64 g, 10 mmol) were dissolved in methanol solution, then reflexed overnight after 5 drops of acetic acid was added. The white product was collected by filtration and washed with methanol several times. Yield: 3.09 g, 82 %. ^{1}H NMR ($CDCl_3$, 400 MHz, *ppm*): 3.92 (s, 3H, $COOCH_3$), 3.97 (d, *J* = 3.4 Hz, 6H, $COOCH_3$), 7.52 (d, *J* = 1.2 Hz, 1H, ArH), 7.92-8.07 (m, 3H, ArH), 8.09 (d, *J* = 1.4 Hz, 1H, ArH), 8.19 (dd, *J* = 14.9, 8.2 Hz, 2H, ArH), 8.58 (s, 1H, CH).

Dimethyl 5-(4-(methoxycarbonyl)benzylamino)isophthalate (b): (E)-dimethyl 5-(4-(methoxycarbonyl) benzylideneamino)isophthalate (1.77 g, 5 mmol) and $NaBH_4$ (0.23 g, 6 mmol) was added to the solution of dichloromethane (30 mL) and methanol (20 mL). After being stirred for 10

h at the room temperature, diluted HCl (1.0 mol) was added to the solution to quench the reaction. Organic solvent was evaporated in vacuum and the pH value of the rest aqueous was adjusted to 8~10 with a saturated solution of sodium bicarbonate, and then extracted with ethyl acetate to the crude desired compound as solid. The residue was purified by silica gel column chromatography (ethyl acetate/dichloromethane, 1:100 as an eluent). Yield: 1.42 g, 79 %. ^{1}H NMR ($CDCl_3$, 400 MHz, *ppm*): 3.90 (s, 6H, $COOCH_3$), 3.91 (s, 3H, $COOCH_3$), 4.48 (s, 2H, CH_2), 7.43 (d, *J* = 8.3 Hz, 2H, ArH), 7.46 (d, *J* = 1.4 Hz, 2H, ArH), 7.98-8.06 (m, 3H, ArH).

5-(4-(hydrazinecarbonyl)benzylamino)isophthalohydrazide (c): A mixture solution of 80 % hydrazine hydrate (5.25 g, 84 mmol) and dimethyl 5-(4-(methoxycarbonyl)benzylamino)isophthalate (0.5 g, 1.40 mmol) in methanol (30 mL) was stirred over 12 h at 70 °C. The precipitate was collected by filtration, washed with methanol and dried in vacuum. Yield: 0.36 g, 72 %. ^{1}H NMR (DMSO-d_6, 400 MHz, *ppm*): 4.39 (d, *J* = 6.0 Hz, 2H, CH_2), 4.49 (d, *J* = 39.9 Hz, 6H, NH_2), 7.10 (s, 1H, ArH), 7.32-7.44 (m, 2H, ArH), 7.48 (d, *J* = 7.8 Hz, 1H, ArH), 7.76 (d, *J* = 8.2 Hz, 2H, ArH), 9.55 (s, 2H, CONH), 9.71 (s, 1H, CONH).

Ligand YL: 5-(4-(hydrazinecarbonyl)benzylamino)isophthalohydrazide (0.5 g, 1.40 mmol) was added to a methanol solution (40 mL) containing 2-pyridinecarboxaldehyde (0.495 g, 4.62 mmol). After 5 drops of acetic acid was added, the mixture was reflexed overnight at 70 °C. The yellow product was collected by filtration, washed with methanol and dried in vacuum. Yield: 0.67 g, 70 %. Anal calc. For $C_{36}H_{28}N_{10}O_3$: H 4.35, C 66.65, N 21.59 %. Found: H 4.40, C 66.89, N 21.32 %. ^{1}H NMR (DMSO-d_6, 400 MHz, *ppm*): 3.83 (s, 1H, NH), 4.51 (d, *J* = 4.7 Hz, 2H, CH_2), 7.00 (s, 1H, CH=N),7.30 (d, *J* = 10.0 Hz, 2H, CH=N), 7.48-7.34 (m, 3H, ArH),7.54 (t, *J* = 9.4 Hz, 2H, ArH), 7.62 (s, 1H, ArH), 7.93 (s, 4H, ArH), 7.96 (t, *J* = 11.0 Hz, 3H, ArH), 8.44 (s, 1H, ArH), 8.47 (d, *J* = 11.3 Hz, 2H, ArH), 8.61 (d, *J* = 4.4 Hz, 3H, ArH), 12.01 (s, 1H, CONH), 12.08 (s, 2H, CONH).

Ni–YL: A mixture of $Ni(BF_4)_2{\cdot}6H_2O$ (0.051 g, 0.150 mmol) and ligand **YL** (0.093 g, 0.150 mmol) was dissolved in 20 mL acetonitrile with strong stirring at 60 °C for 2 h. Then the solution was filtrated after cooled to room temperature. Reddish block crystals were obtained through diffusing diethyl ether into the above filtrate after one week. Yield: 62 % (based on the crystal dried in vacuum). Anal calc. For $Ni_6(C_{204}H_{164}N_{60}O_{18})(BF_4)_8(CH_3CN)_3(H_2O)_7$: H 3.74, C 50.04, N 17.51 %. Found: H 3.93, C 50.78, N 17.23 %.

Ni–ML: Phenylamine (0.028 g, 0.3 mmol), 2-pyridinecarboxaldehyde (0.032 g, 0.3 mmol) and $Ni(BF_4)_2{\cdot}6H_2O$ (0.034 g, 0.10 mmol) were dissolved in 20 mL acetonitrile. The reaction mixture was reflexed for one day at 70 °C. Then cooling to room temperature, brown sliced crystals were obtained through diffusing diethyl ether into the above solution after two weeks. Yield: 65 %. Anal calc. For $Ni(C_{36}H_{30}N_6)(BF_4)_2(H_2O)_{0.5}$: H 3.96, C 54.87, N 10.66 %. Found: H 3.88, C 55.02, N 9.74 %.

Crystallography

X-Ray intensity data were measured at 200(2) K on a Bruker SMART APEX CCD-based diffractometer (Mo–Kα radiation, λ = 0.71073 Å) using the SMART and SAINT programs.[28,29] The crystal data was solved by direct methods and further refined by full-matrix least-squares refinements on F^2 using the SHELXL-97 software and an absorption correction was performed using the SADABS program.[30] Non-H atoms were refined with anisotropic displacement parameters. The hydrogen atoms within the ligand backbones and the solvent CH_3CN molecules were fixed geometrically at calculated distances and allowed to ride on the parent non-hydrogen atoms. For Ni–**YL**, four fluorine atoms in two half occupied BF_4^- ions were disordered into two parts with each S. O. F. (site occupied factor) fixed as 0.25. The B-F bond distances and F-F distances of several BF_4^- ions were constrained to be same, and the thermal parameters of adjacent atoms in these BF_4^- ions were constrained to be similar. For Ni–**ML**, three F atoms in BF_4^- ions were disordered into two parts with each S. O. F. fixed as 0.5. The crystal data were listed in Table 1.

Table 1. The crystal data of Ni–**YL** and Ni–**ML**

Compounds	Ni–**YL**	Ni–**ML**
Empirical formula	$C_{210}H_{187}N_{63}O_{25}Ni_6B_8F_{32}$	$C_{36}H_{31}N_6O_{0.5}NiB_2F_8$
Formula weight	5039.97	788.00
T/K	200(2)	200(2)
Crystal system	Orthorhombicl	Triclinic
Space group	*Fdd*2	*P*-1
a/Å	62.337(8)	9.6501(12)
b/Å	18.920(2)	19.591(2)
c/Å	54.815(7)	20.506(3)
α/°	90	113.857(9)
β/°	90	95.885(9)
γ/°	90	90.008(9)
V/Å^3	64651(14)	3523.1(7)
Z	8	4
D_{calc}/Mg m^{-3}	1.035	1.486
μ/mm^{-1}	1.035	0.632
F(000)	20656	1612
R_{int}	0.1229	0.0980
Data/parameters	28367 / 1781	12116 / 992
GOF	0.974	0.992
R [$I > 2\sigma(I)$][a]	R_1 = 0.0906 wR_2 = 0.1941	R_1 = 0.0874 wR_2 = 0.1727
R indices (all data)[b]	R_1 = 0.1901 wR_2 = 0.2244	R_1 = 0.1767 wR_2 = 0.1937
$\Delta\rho_{max,min}$/eÅ^{-3}	0.573 / -0.359	0.925 / -0.881
CCDC number	1063216	1063217

[a] $R_1 = \Sigma||F_o| - |F_c||/\Sigma|F_o|$; [b] $wR_2 = \Sigma[w(F_o^2 - F_c^2)^2]/\Sigma[w(F_o^2)^2]^{1/2}$

Acknowledgements

We gratefully acknowledge financial support from the NSFC (21231003 and 21531001), and the Program for Changjiang Scholars and Innovative Research Team in University (IRT1213).

Keywords: metal-organic cylinder • encapsulation • ruthenium(II) complex • photoinduced electron transfer (PET) • hydrogen production

[1] R. F. Ludlow, S. Otto, *Chem. Soc. Rev*. **2008**, *37*, 101–108.
[2] S. Zarra, D. M. Wood, D. A. Roberts, J. R. Nitschke, *Chem. Soc. Rev*. **2015**, *44*, 419–432.

[3] a) W. M. Hart-Cooper, K. N. Clary, F. D. Toste, R. G. Bergman, K. N. Raymond, *J. Am. Chem. Soc*. **2012**, *134*, 17873–17876; b) Q. Zhang, K. Tiefenbacher, *J. Am. Chem. Soc*. **2013**,*135*, 16213–16219; c) Y. Jiao, J. Wang, P. Y. Wu, L. Zhao, C. He, J. Zhang, C. Y. Duan, *Chem. – Eur. J*. **2014**, *20*, 2224–2231.

[4] Examples for the organic macrocycles hosts: a) P. Mukhopadhyay, A. X. Wu, L. Isaacs, *J. Org. Chem*. **2004**, *69*, 6157–6164; b) W. Jiang, D. Ajami, J. Rebek, Jr. *J. Am. Chem. Soc*. **2012**, *134*, 8070–8073; c) H. Y. Gan, B. C. Gibb, *Chem. Commun*. **2012**, *48*, 1656–1658; d) A. Ikeda, S. Shinkai, *Chem. Rev*. **1997**, *97*, 1713–1734; e) T. Brotin, J. P. Dutasta, *Chem. Rev*. **2009**, *109*, 88–130; f) M. N. Berberan-Santos, P. Choppinet, A. Fedorov, L. Jullien, B. Valeur, *J. Am. Chem. Soc*. **2000**, *122*, 11876–11886; g) E. A. Meyer, R. K. Castellano, F. Diederich, *Angew. Chem. Int. Ed*. 2**003**, *42*, 1210–1250.

[5] a) M. Yoshizawa, M. Tamura, M. Fujita, *Science*, **2006**, *312*, 251–254; b) P. Mal, B. Breiner, K. Rissanen, J. R. Nitschke, *Science*, **2009**, *324*, 1697–1699; c) M. D. Pluth, R. G. Bergman, K. N. Raymond, *Science*, **2007**, *316*, 85–88.

[6] a) A. Jiménez, R. A. Bibeisi, T. K. Ronson, S. Zarra, C. Woodhead, J. R. Nitschke, *Angew. Chem. Int. Ed*. 2**014**, *53*, 4556–4560; b) K. Mahata, P. D. Frischmann, F. Würthner, *J. Am. Chem. Soc*. **2013**, *135*, 15656–15661; c) C. J. Hastings, M. P. Backlund, R. G. Bergman, K. N. Raymond, *Angew. Chem. Int. Ed*. **2011**, *50*, 10570–10573; d) D. M. Kaphan, F. D. Toste, R. G. Bergman, K. N. Raymond, *J. Am. Chem. Soc*. **2015**, *137*, 9202–9205; e) M. Otte, P. F. Kuijpers, O. Troeppner, I. Ivanović-Burmazović, J. N. H. Reek, B. de Bruin, *Chem. – Eur. J*. **2014**, *20*, 4880–4884; f) A. H. Chughtai, N. Ahmad, H. A. Younus, A. Laypkov, F. Verpoort, *Chem. Soc. Rev*. **2015**, *44*, 6804–6849.

[7] a) M. L. Singleton, J. H. Reibenspies, M. Y. Darensbourg, *J. Am. Chem. Soc.* **2010**, *132*, 8870–8871; b) G. Ghale, V. Ramalingam, A. R. Urbach, W. M. Nau, *J. Am. Chem. Soc*. **2011**, *133*, 7528–7535; c) X. Jing, C. He, Y. Yang, C. Y. Duan, *J. Am. Chem. Soc*. **2015**, *137*, 3967–3974.

[8] P. D. Frischmann, K. Mahata, F. Würthner, *Chem. Soc. Rev*. **2013**, *42*, 1847–1870.

[9] C. K. Prier, D. A. Rankic, D. W. C. MacMillan, *Chem. Rev*. **2013**, *113*, 5322–5363.

[10] a) C. He, Z. H. Lin, Z. He, C. Y. Duan, C. H. Xu, Z. M. Wang, C. H. Yan, *Angew. Chem. Int. Ed*. **2008**, *47*, 877–881; b) H. M. Wu, C. He, Z. H. Lin, Y. Liu, C. Y. Duan, *Inorg. Chem*. **2009**, *48*, 408–410.

[11] a) A. M. Stadler, J. Harrowfield, *Inorg. Chim. Acta*, **2009**, *362*, 4298–4314; b) L. Zhao, S. Y. Qu, C. He, R. Zhang, C. Y. Duan, *Chem. Comm*. **2011**, *47*, 9387–9389.

[12] K. I. Assaf, W. M. Nau, *Chem. Soc. Rev*. **2015**, *44*, 394–418.

[13] J. Lagona, P. Mukhopadhyay, S. Chakrabarti, L. Isaacs, *Angew. Chem. Int. Ed*. **2005**, *44*, 4844–4870.

[14] a) H. Tang, D. Fuentealba, Y. H. Ko, N. Selvapalam, K. Kim, C. Bohne, *J. Am. Chem. Soc*. **2011**, *133*, 20623–20633; b) S. Ghosh, P. Mukhopadhyay, L. Isaacs, *J. Syst. Chem*. **2010**, *1*, 6.

[15] a) A. K. Rappé, C. J. Casewit, K. S. Colwell, W. A. G. III, W. M. Skiff, *J. Am. Chem. Soc*. **1992**, *114*, 10024–10035; b) Gaussian 09, Revision B.01, M. J. Frisch, G. W. Trucks, H. B. Schlegel, G. E. Scuseria, M. A. Robb, J. R. Cheeseman, G. Scalmani, V. Barone, B. Mennucci, G. A. Petersson, H. Nakatsuji, M. Caricato, X. Li, H. P. Hratchian, A. F. Izmaylov, J. Bloino, G. Zheng, J. L. Sonnenberg, M. Hada, M. Ehara, K. Toyota, R. Fukuda, J. Hasegawa, M. Ishida, T. Nakajima, Y. Honda, O. Kitao, H. Nakai, T. Vreven, J. A. Montgomery, Jr., J. E. Peralta, F. Ogliaro, M. Bearpark, J. J. Heyd, E. Brothers, K. N. Kudin, V. N. Staroverov, T. Keith, R. Kobayashi, J. Normand, K. Raghavachari, A. Rendell, J. C. Burant, S. S. Iyengar, J. Tomasi, M. Cossi, N. Rega, J. M. Millam, M. Klene, J. E. Knox, J. B. Cross, V. Bakken, C. Adamo, J. Jaramillo, R. Gomperts, R. E. Stratmann, O. Yazyev, A. J. Austin, R. Cammi, C. Pomelli, J. W. Ochterski, R. L. Martin, K. Morokuma, V. G. Zakrzewski, G. A. Voth, P. Salvador, J. J. Dannenberg, S. Dapprich, A. D. Daniels, O. Farkas, J. B. Foresman, J. V. Ortiz, J. Cioslowski, and D. J. Fox, Gaussian, Inc., Wallingford CT, **2010**.

[16] A. D. Wilson, R. H. Newell, M. J. McNevin, J. T. Muckerman, M. R. DuBois, D. L. DuBois, *J. Am. Chem. Soc*. **2006**, *128*, 358–366.

[17] K. Swarnalatha, E. Rajkumar, S. Rajagopal, R. Ramaraj, Y. L. Lu, K. L. Lu, P. Ramamurthy, *J. Photoch. Photobio. A*, **2005**, *171*, 83–90.

[18] a) E. Rajkumar and S. Rajagopal, *Photochem. Photobiol. Sci*. **2008**, *7*, 1407–1414; b) J. I. Goldsmith, W. R. Hudson, M. S. Lowry, T. H. Anderson, S. Bernhard, *J. Am. Chem. Soc*. **2005**, *127*, 7502–7510.

[19] D. Thiruppathi, P. Karuppasamy, M. Ganesan, V. K. Sivasubramanian, T. Rajendran, S. Rajahopal, *J. Photoch. Photobio. A*, **2014**, *295*, 70–78.

[20] R. J. Holbrook, D. J. Weinberg, M. D. Peterson, E. A. Weiss, T. J. Meade, *J. Am. Chem. Soc*. **2015**, *137*, 3379–3385.

[21] H. F. M. Nelissen, M. Kercher, L. De Cola, M. C. Feiters, R. J. M. Nolte, *Chem.-Eur. J*. **2002**, *8*, 5407–5414.

[22] M. P. McLaughlin, T. M. McCormick, R. Eisenberg, P. L. Holland, *Chem. Commun*. **2011**, *47*, 7989–7991.

[23] C. He, J. Wang, L. Zhao, T. Liu, J. Zhang, C. Y. Duan, *Chem. Commun*. **2013**, *49*, 627–629.

[24] C. J. Hastings, D. Fiedler, R. G. Bergman, K. N. Raymond, *J. Am. Chem. Soc*. **2008**, *130*, 10977–10983.

[25] S. Q. Zhang, L. Han, L. N. Li, J. Cheng, D. Q. Yuan, J. H. Luo, *Cryst. Growth Des*. **2013**, *13*, 5466–5472.

[26] C. M. Elliott, *Langmuir*, **2005**, *21*, 3022–3027.

[27] P. Zhang, M. Wang, Y. Na, X. Li, Y. Jiang, L. Sun, *Dalton Trans.* **2010**, *39*, 1204–1206.

[28] *SMART Data collection software*, version 5.629; Bruker AXS Inc.: Madison, WI, **2003**.

[29] *SAINT Data reduction software*, version 6.45; Bruker AXS Inc.: Madison, WI, **2003**.

[30] G. M. Sheldrick, *SHELX-97: Program for crystal structure analysis*; University of Göttingen: Göttingen, Germany, **1997**.

FULL PAPER

Supramolecular encapsulation behavior of the size-suitable anionic $Ru(dcbpy)_3$ within the cavity of hexanuclear metal-organic cylinder host was investigated. The supramolecular system improved a pseudo intramolecular PET process and gave rise to the well-emerged new reaction pathways of H_2 production.

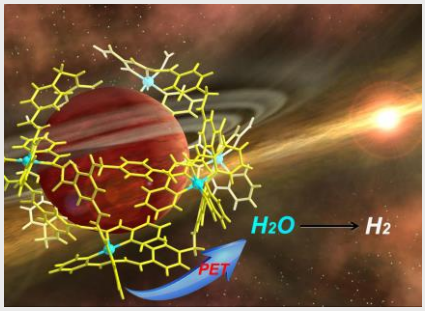

Lu Yang, Cheng He, Xin Liu, Jing Zhang, Hui Sun and Huimin Guo**

Page No. – Page No.

Supramolecular Photoinduced Electron Transfer between A Redox-active Hexanuclear Metal-organic Cylinder and Encapsulated Ruthenium(II) Complex